ISSN 0915-633X

NATIONAL INSTITUTE FOR FUSION SCIENCE

Properties of Turbulence and Stationary Zonal Flow on Transport Barrier in CHS

A. Fujisawa, A. Shimizu, H. Nakano, S. Ohsima, K. Itoh, H. Iguchi,
K. Matsuoka, S. Okamura, S.-I. Itoh and P.H. Diamond

(Received - Sep. 26, 2005)

NIFS-824 Oct. 2005

RESEARCH REPORT
NIFS Series

TOKI, JAPAN

Properties of turbulence and stationary zonal flow on transport barrier in CHS

A. Fujisawa, A. Shimizu, H. Nakano, S. Ohsima, K. Itoh, H. Iguchi, K. Matsuoka, S. Okamura, S.-I. Itoh[1] and P. H. Diamond[2]

National Institute for Fusion Science, Oroshi-cho, Toki-shi, 509-52 Japan
[1]RIAM, Kyushu Univ., Kasuga 816 Japan
[2]University of California, San Diego, La Jolla, California, United States of America

Abstract. Spectral changes in electric field fluctuation are measured using twin heavy ion beam probes in CHS before and after an internal transport barrier is broken down. A wavelet analysis reveals intermittent behaviors of the fluctuations, and a significant correlation between fluctuation powers of the low ($2.5 < f < 10$ kHz) and high ($30 < f < 250$ kHz) ranges. The high frequency (turbulence) fluctuation increases with a decrease in the low frequency fluctuation after the back-transition. The change in the power distribution between these two frequency ranges may contribute to the improved transport on the barrier.

Keywords; electric field fluctuation, heavy ion beam probes, turbulence, zonal flow, internal transport barrier

1. Introduction

The cause of transport barriers[1, 2] has been ascribed to formation of sheared radial electric field (or flow perpendicular to magnetic field) which results in the turbulence and transport reduction[3, 4]. Recent simulation and theoretical works have suggested an important role of mesoscopic structure of electric field, termed zonal flows[5, 6, 7]. Full understanding of plasma transport requires investigation of interplay between electric field fluctuation of three different scales, *i. e.,* turbulence, zonal and mean flows. In a recent experiment in CHS, twin heavy ion beam probes (HIBP) succeeded to identify the existence of zonal flow[8] and to observe the electric field fluctuations in high temperature core. This paper reports the result of the direct measurements of electric field fluctuations on an internal transport barrier (ITB) and an interplay between the fluctuations in disparate scales.

2. Experimental Set-up

2.1. Compact Helical System

Compact Helical System (CHS) is a toroidal helical device of which the major and averaged minor radii are $R = 1$ m and $a = 0.2$ m, respectively. A pair of helical coils generates the confinement magnetic field that has periodicity of m=2 and n=8

in poloidal and toroidal direction, respectively. Four pairs of poloidal field coils are equipped to control magnetic axis and to shape magnetic field cage, such as ellipticity and triangularity. Two neutral beam injection (NBI) systems and two gyrotrons are used as heating apparatus. Combination of these heating methods allows a wide choice of plasma parameters. CHS has two HIBPs located in different toroidal positions by 90° apart. The system of twin HIBPs allows us to investigate both local and global characteristics of turbulence.

Each HIBP is equipped with three channels, $\delta\phi(r-\delta r)$, $\delta\phi(r)$ and $\delta\phi(r+\delta r)$, to simultaneously observe the potentials at adjacent spatial points of the plasma. Potential is an integral of electric field, and its fluctuation is described as $\delta\phi(r) = \delta\phi_{\rm local} + \delta\phi_{\rm path}$, where the first and second parts are symbolically written as $\delta\phi_{\rm local} = \delta E\delta l$ and $\delta\phi_{\rm path} = \int \delta E dl$. The potential at the observation point located in the upper stream $\delta\phi(r-\delta r)$ is considered to be equivalent to $\delta\phi_{\rm path}$, therefore, the local fluctuation or electric field fluctuation can be evaluated from the potential difference between two of the three local channels; for example, $\delta\phi(r) - \delta\phi(r+\delta r) = \delta\phi_{\rm local}$.

The Gabour's wavelet (or Milligen's) is used to extract the temporal evolution of electric field fluctuation. The wavelet is a natural extension of the traditional Fourier transformation. The transformation is defined as $F(f,t) = \int_{-\infty}^{\infty} f(\tau)\Phi(f,t-\tau)d\tau$ with $\Phi(f,t) = \sqrt{f}\exp[i2\pi ft - (ft)^2/2]$. The auto-power is evaluated using the following formula, $P_{\rm auto} = \int_{t-T}^{t+T} F(f,\tau)F^*(f,\tau)d\tau/2T$, where the integral takes over a finite period of T. In the following analysis, the period of T is chosen to be 0.25 ms, or temporal evolution of fluctuation at a frequency is resolved in every 0.1 ms. The integral is simplified to summation of discrete time τ_i. The interval of neighboring ensemble time is set as $\tau_i = 1/2f$. Note that the uncertain principle $\Delta f\Delta t \sim 1$ gives a limitation of simultaneous resolutions in time and frequency to the time-dependent Fourier analysis.

3. Experimental Resutls

3.1. Potential and Density during Transition

The target plasma is produced with electron cyclotron resonance (ECR) heating of $\sim$ 200 kW. The chosen plasma parameters were, magnetic field strength $B = 0.88$ T, density $n_{\rm e} \simeq 4\times10^{12}{\rm cm}^{-3}$, electron temperature $T_{\rm e} \simeq 1$ keV, and ion temperature $T_{\rm i} \simeq 0.1$ keV. In the discharge condition, the internal transport barrier is generated[9] and a back-transition often takes place in the later phase of the discharges. The measurements using the twin HIBP are performed on the discharges and happen to catch the exact moment of the transition. The necessary beam energy is $\sim$70 keV for the experimental condition of the magnetic field strength. The sampling rate of the HIBP signals is 2 μs, giving to the Nyquist frequency of 250 kHz.

Figure 1 is an example of potential waveforms to indicate the back-transition from the state with the ITB to the one without. The first HIBP potential (the solid line) indicates the timing of the back-transition by a sharp drop at $t \sim 71.4$ ms, while the second HIBP potential shows no significant change at the moment. The observation point of the second HIBP is inferred to be located exactly at the barrier foot point, while the first one is inside the barrier. This conclusion is derived from the following facts.

From the previous experiments, the width of the barrier region (or effective $E_{\rm r}$-shear layer) is supposed to be $\sim$ 1.5 cm[9]. In the series of discharges of the experiment

a significant potential drop of the second HIBP ($\sim$ 30 V) was observed when the observation point was moved inward by 1 cm. This means that the position of 1 cm inside should be out of the effective shear layer, hence, the observation point of the second HIBP is localized in the barrier position.

In addition, the detected beam current of the second HIBP exhibits a peculiar behavior. Figure 1b shows the signals of three channels. The signals from inside and center channels indicate sharp rises at the time of transition, while the outside channel does not show an increase. A trajectory calculation including a finite diameter of the beam shows that the observation radii of the three channels are $r_{\rm in} = 6.0$, $r_{\rm cen} = 6.4$ and $r_{\rm out} = 7.0$ cm, and the distances between center and top and between center and bottom are 5 mm, and 8 mm, respectively. These facts support that the center channel should be located at the center of the barrier foot point region within the approximate error of $\sim$ 5 mm.

3.2. Electric Field Fluctuation around Internal Transport Barrier

The wavelet analysis is performed on electric field fluctuation. Figure 2a shows evolution of the spectrum of $E\delta l = \delta\phi(r_{\rm cen}) - \delta\phi(r_{\rm out})$. The image plot shows that *turbulence* power in higher frequency than 30 kHz clearly increases being accompanied with the expansion of turbulence frequency range after the barrier is lost. The image plot also visualizes the intermittent activity of fluctuation at 20 kHz, which disappears after the back-transition. The total and integrated fluctuation powers in two frequency ranges are demonstrated in Fig. 2b. The fluctuation power in the frequency range of $2.5 < f < 10$ kHz decreases in the averaged value after the transition, while the that in the frequency range of > 30 kHz indicates a clear increase. The change in the total power of the electric field fluctuation (precisely the local potential difference) corresponds to the increase from $\sim$ 5V to $\sim$ 7V in amplitude.

The spectra and coherence are evaluated using the traditional fast Fourier transformation in oder to obtain the statistical properties of fluctuations, particularly for low frequency range; a longer temporal window (than 1 ms) is necessary to estimate the properties of low frequency fluctuation of a few kHz. Figure 3 shows the spectra of electric field fluctuation at the barrier and with coherences between two toroidal locations before and after the back-transition. The comparison of the spectra confirms that broad-band turbulence power around $\sim$ 60 kHz increases after the transition, while the low frequency power of $2.5 < f < 10$ kHz decreases. In addition, two obvious peaks at $\sim$ 20 and $\sim$ 40 kHz are found to be lost after the transition.

The coherence analysis shows no significant correlation in the frequency higher than 10 kHz. However, a significant coherence between two toroidal locations is found in the region less than 10 kHz. The coherence value increases up to 0.8 at $\sim$ 2 kHz in the state with the barrier, although the value is smaller ($\sim$ 0.5) in the state without barrier. The long-distance correlation suggests that the electric field fluctuation in the low frequency range should be associated with zonal flows.

3.3. Interplay between fluctuations

The spectral analysis suggests that the electric field fluctuation could be divided into three parts; i) low frequency region less that 10 kHz characterized with long-distance correlation, ii) turbulence region above 30 kHz characterized with a broad-band peak, and iii) an intermediate frequency region which indicates a valley in the fluctuation

power without long-distance correlation.

The wavelet analysis allows us to estimate temporal behavior of the three frequency ranges. Figure 4 shows the normalized powers of the three frequency ranges. Here, the normalized power is defined as $q(f_{\rm l}, f_{\rm h}) = \int_{\rm f_l}^{\rm f_h} P(f)df / \int_0^\infty P(f)df$, where$P(f)$ and $q(f_{\rm l}, f_{\rm h})$ means the power density at the frequency f and the power fraction of the frequency range from $f_{\rm l}$ to $f_{\rm h}$, respectively. As is shown in Fig. 4a, the two powers evolve in a manner of anti-phase. In other words, one increases accompanied with the other decrease. This tendency is obvious particularly before the transition.

Figure 4c shows the statistical analysis for the correlation between normalized powers of the three frequency ranges in the state with the barrier. Here, the normalized powers of turbulence and the intermediate frequency range are plotted as a function of the normalized power of the low frequency. A simple regression analysis shows a linear relationship between turbulence and low frequency powers, while no significant correlation is found between intermediate and lower frequency. The relations are explicitly written as $q(250, 30) \simeq 0.89 - q(2.5, 30)$ and $q(30, 10) \simeq 0.11$. The relation suggests the direct energy exchange between fluctuations of high and low frequency ranges.

4. Discussion and Summary

The low frequency range fluctuation shows that the long-distance correlation between two toroidal locations. This property suggests that the frequency range activity should reflect stationary zonal flow, although the strict identification needs confirmation of radial structure. The simple statistical analysis in Fig. 4 implies a significant links between power fractions of turbulence and lower frequency fluctuation, suggesting a causal link between zonal flow and turbulence. In addition, the difference distribution of power fraction is found for the states with and without a barrier. The fact suggests that the higher fraction of the low frequency power should contribute to transport improvement in the state with a barrier, since the fluctuation with lower frequency, at least, is expected to correspond to smaller poloidal wave number.

In the intermediate frequency range, two sharp peaks at 20 and 40 kHz are found in the spectrum of electric field fluctuation at the barrier (the first HIBP). At the frequencies, no long-distance correlation between two toroidal locations is found in electric field fluctuations , however, the significant coherence is obtained in the coherence between the electric fluctuation and the potential fluctuation. The modes should be localized in an outer region of the barrier and the potential fluctuation, which is an integrated fluctuation, should sense the fluctuation along the beam orbit , then give a significant value of coherence. No significant correlation with magnetic field fluctuation is found at these two frequencies, hence, the modes show electrostatic characteristics in the global sense. Consequently, the electrostatic characteristics and long-distance property suggest that the modes could be geodesic acoustic modes (GAMs)[12, 13, 14].

In summary, the experimental results demonstrate difference in spectra of electric field fluctuation at a barrier position with and without a transport barrier. The distribution ratio changes between fluctuation powers of low and higher frequency ranges. In the state with a barrier, a larger fraction of low frequency power may contribute to the improvement at the barrier transport. A significant correlation

between the turbulence and low frequency fluctuation power is found to suggest a causal link between zonal flow and turbulence.

Acknowledgements

This work is partly supported by the Grant-in-Aids for Scientific Research (No. 15360497) and Specially-Promoted Research (No.16002005). The authors are grateful to Prof. O. Motojima for his continuous supports and encouragements.

References

[1] F. Wagner et al., Phys. Rev. Lett. **49** 1408 (1982).
[2] A. Fujisawa, Plasma Phys. Control. Fusion **45** R1 (2003).
[3] H. Biglari, P. H. Diamond, P. W. Terry, Phys. Fluids B **2** 1 (1990).
[4] K. Itoh, S.-I. Itoh, A. Fukuyama, H. Sanuki, M. Yagi, Plasma Phys. Control. Fusion **36** 123 (1994).
[5] P. H. Diamond, K. Itoh, S.-I. Itoh, T. S. Hahm, Plasma Phys. Control. Fusion **47** R35 (2005).
[6] M. N. Rosenbluth, F. L. Hinton, Phys. Rev. Lett. **80**, 724 (1998).
[7] N. Winsor, J. L. Johnson, and J. M. Dawson, Phys. Fluids 11, 2448 (1968).
[8] A. Fujisawa et al., Phys. Rev. Lett. **93** 165002 (2004).
[9] A. Fujisawa et al., Phys. Rev. Lett. **82** 2669 (1999).
[10] B. Ph. van Milligen, C. Hidalgo, E. Sanchez, Phys. Rev. Lett. **74** 395 (1995).
[11] K. Hallatschek, D. Biskamp, Phys. Rev. Lett. **86** 1223 (2001).
[12] T. Watari, Y. Hamada, A. Fujisawa, K. Toi, K. Itoh, Phys. of Plasmas **12** 062304 (2005).
[13] M. G. Shats, W. M. Solomon, Phys. Rev. Lett. **88**, 045001 (2002).
[14] G. R. McKee, *et al.*, Plasma Phys. Control. Fusion **45**, A477 (2003).

Figure 1. Signals of heavy ion beam probes. (a) Potential signals of twin HIBPs which are located in different toroidal locations. The first HIBP potential indicates an exact time of a back-transition, while the second one shows no significant change. (b) The signals of detected beam current in three detectors of the second HIBP. The difference between three signals at the transition moment implies that the center channel should be located exactly in the effective shear layer of the barrier.

Figure 2. (a)Temporal evolutions of wavelet power spectrum of electric field fluctuation. (b) Temporal evolution of electric field fluctuation powers in frequency ranges of $2.5 < f < 10$ kHz and $30 < f < 250$ kHz. The total power is indicated by a thin grey line.

Figure 3. Spectral difference in electric field fluctuation on the barrier before and after the transition. (b) Coherences of electric field fluctuations between two torooidal locations before and after the transition.

Figure 4. (a) Temporal evolution of fluctuation power fractions $q(30, 250)$ and $q(2.5, 10)$, where $q(f_L, f_H)$ are the power fraction in the frequency ranges of $f_L < f < f_H$ kHz. The dashed line represents $q(2.5, 10) = 0.89 - q(30, 250)$. (b) Temporal evolution of fluctuation power fraction of intermediate range of $10 < f < 30$ kHz. (c) Power fractions of intermediate $q(10, 30)$ and higher frequency $q(30, 250)$ as a function of power fraction of the low frequency $q(2.5, 10)$.

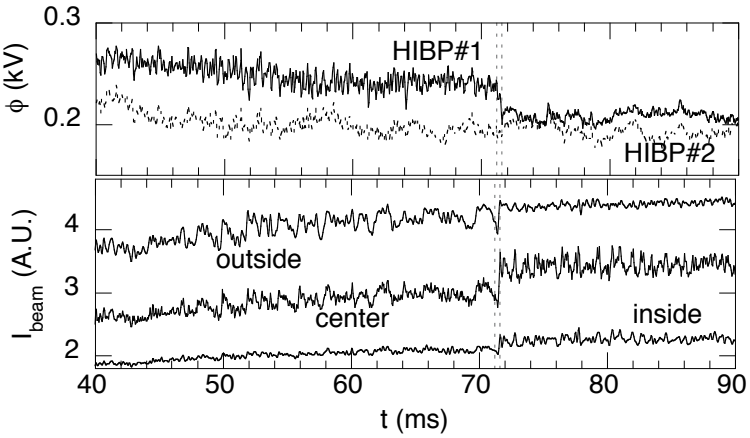

Figure 1 A. Fujisawa et al.

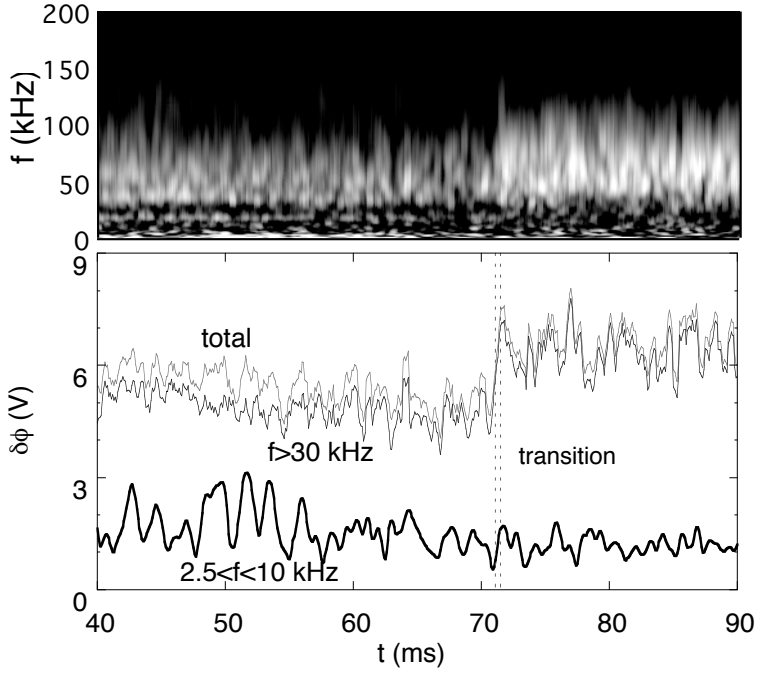

Figure 2 A. Fujisawa et al.

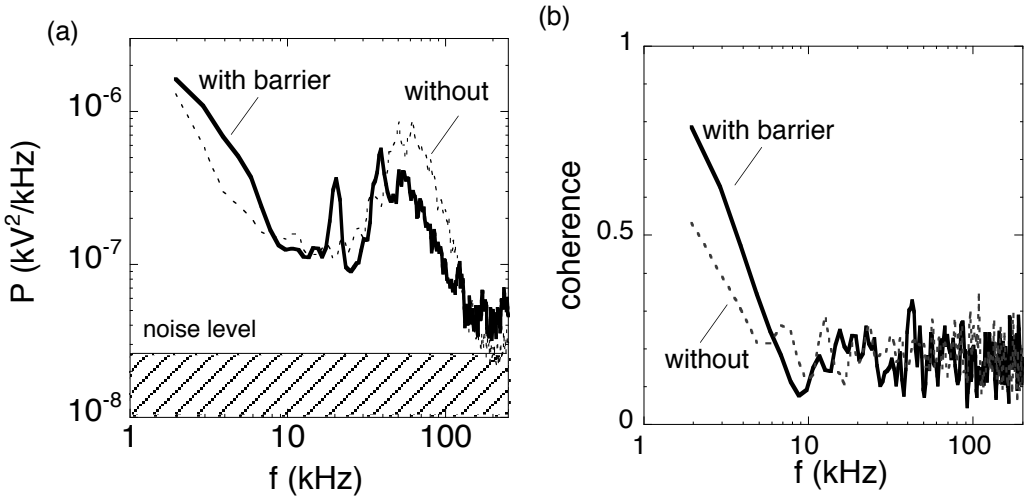

Figure 3 A. Fujisawa et al.

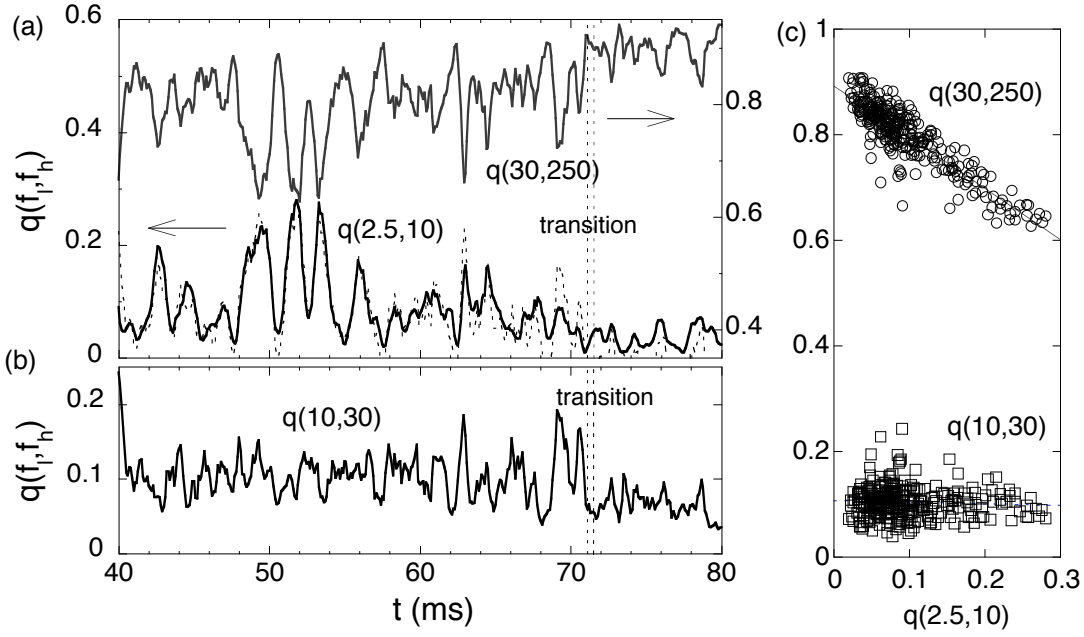

Figure 4 A. Fujisawa et al.